Image Cover Sheet

CLASSIFICATION	SYSTEM NUMBER 131298
UNCLASSIFIED	

TITLE

THE APPLICATION OF A RADIAL BASIS FUNCTION NEURAL NETWORK FOR RADAR TRACKING OVER THE SEA

System Number:

Patron Number:

Requester:

Notes: Paper #11 contained in Parent Sysnum #129006

DSIS Use only:

Deliver to: DK

THE APPLICATION OF A RADIAL BASIS FUNCTION NEURAL NETWORK FOR RADAR TRACKING OVER THE SEA

by

Henry Leung and Eloi Bossé

Surface Radar Section
Radar Division
Defence Research Establishment Ottawa
Ottawa, Ontario
Canada K1A 0Z4

Abstract

A low-angle tracking technique based on the use of a radial basis function neural network is presented. Computer simulations show that the new technique is capable of tracking both stationary and moving targets under low signal-to-noise ratio situations with a high accuracy. As well, the performance of the new technique is tested using real-life data. The results demonstrate the robustness and effectiveness of the new algorithm in terms of its independence of array errors and of the nature of the noise background.

1 Introduction

For decades, a considerable amount of research has been devoted to a near-classic problem which is commonly referred to as "low-angle radar tracking". It is primarily a multipath problem, wherein reflections of radar signals from the sea surface enter the main beam of a shipborne radar and seriously degrade its performance. When the height of a target is such that the angular separation between the direct and indirect paths, along which the radar signal travels from the target to the radar, is less than 0.8 antenna beamwidths (BWs), conventional monopulse techniques will produce large tracking errors.

Because of this limitation of monopulse radars, many signal processing techniques have been developed for tracking low-angle targets. Much of the research work to date has been concentrated in the area of array signal processing, wherein superresolution algorithms have been conceived, developed, tested and accepted or rejected based on their effectiveness and robustness in separating a target from its image and then providing an accurate estimate of the target's angle-of-arrival. Most, if not all, conventional superresolution techniques employed in low-angle radar tracking are based on linear modelling; i.e., the output of a beamformer is linearly related to the outputs of the array antenna. Linear models, in terms of statistics, only make use of the first and second order moment information (e.g. the mean and the variance) of the data. Higher order information is thrown away during the processing. In the case of low-angle tracking, however, the diffuse multipath is described to be coloured and K-distributed [1]. Consequently, these algorithms may not offer a satisfactory performance for low angle tracking over rough sea surfaces.

Accordingly, we introduce a technique which has been developed based on a radial basis function (RBF) neural network [2]. This technique, in conjunction with a comprehensive multipath model, can be used to achieve a resolution that is an order of magnitude greater than that achieved using conventional superresolution processing. In addition, it alleviates the ambiguity problem that other superresolution techniques encounter when a single frequency is used. These significant enhancements are brought about by replacing linear modelling with non-linear modelling.

Recently, neural networks have drawn a lot of attention from the signal processing community

[3,4]. In an attempt to reproduce the capability of a human brain, a neural network consists of a multilayer nonlinear network that is able to decode the higher order information contained in the input data. A neural network tries to reproduce human intellectual capabilities through a "learning" process in which the error between the input-output pair is minimized by varying the weights of the interconnections between the input and output layers. Here, the RBF neural network is applied to low-angle target tracking. The advantages of using an RBF network are twofold. First, it is capable of performing an accurate multivariate approximation even in an ill-posed environment. Second, the optimal weights in the RBF network can be estimated in a linear fashion, and hence is has a much faster convergent rate for learning than many other neural net structures such as the backpropagation multilayer network[4].

2 The Tracking Technique Based on RBF

The signal model to be used here is mainly based on the one described in [5]. This model makes use of geometrical information and a priori knowledge of a number of other physical parameters. These parameters include the refractivity gradient, the reflection coefficient, the specular and diffuse scattering coefficients, and the divergence factor. In order to be consistent with our experimental setup, a bistatic radar signal model is considered. The model is based on one-way transmission, which, despite its simplicity, is useful for testing the performance of spectral estimation techniques and is suitable for carrying out experimental investigations. It is much easier and less expensive to set up a beacon system and a narrow-band receiving array than to implement a radar system with its much more complicated transmission and reception system. The one-way transmission model is easily extended to a two-way model and the wide-band channel can in principle be treated as an ensemble of contiguous narrow-band channels.

The geometry of a simple flat earth model for multipath is illustrated in Fig. 1. By taking into account of the curvature of signal path due to refraction and the curvature of the Earth itself, the received signal at the k^{th} element of the array is given by

$$s_k = \gamma e^{j\varphi} e^{j\kappa[r+(h'-z_k')^2/2r]}\left[1+\rho e^{j(\phi+2\kappa h' z_k'/r)}\right] \qquad (1)$$

where $\kappa = 2\pi / \lambda$ is the wavenumber

$h' \approx h - r_2^2/2R_e$

$z_k' = z_k - r_1^2/2R_e$

$R_e = R\,(1+6.37\times10^{-3}\,dN/dh)^{-1}$

R is earth radius.

In (1), the term $\gamma e^{j\varphi}$ is the complex amplitude of the radar signal and the term $\rho e^{j\phi}$ is the overall reflection coefficient. It generally consists of three factors, namely the reflection coefficient for a plane surface, Γ, the divergence factor due to curved surface, D, and the specular scattering coefficient S; i.e.

$$\rho e^{j\phi} = \Gamma \cdot D \cdot S \tag{2}$$

The approximate expressions for the Fresnel reflection coefficient for a smooth plane surface are given by

$$\Gamma_v \approx \frac{\sqrt{\epsilon_c}\sin\psi - 1}{\sqrt{\epsilon_c}\sin\psi + 1} \tag{3}$$

for vertical polarization and

$$\Gamma_h \approx \frac{\sin\psi - \sqrt{\epsilon_c}}{\sin\psi + \sqrt{\epsilon_c}} \tag{4}$$

for horizontal polarization, where ψ is the grazing angle and ϵ_c is the complex dielectric constant of the reflecting medium. The derivation of the grazing angle is based on the geometrical information. The divergence factor is approximated by

$$D \approx \left[1 + \frac{2r_1 r_2}{R_e r \psi}\right]^{-\frac{1}{2}} \tag{5}$$

The root-mean-squared specular scattering coefficient S is given by

$$S = e^{-\mu} \tag{6}$$

where

$$\mu = \begin{cases} 2[2\pi\eta]^2 & \eta \le 0.1 \ \textit{radian} \\ 0.165\eta^2 + 7.42\eta + 0.0468 & \textit{otherwise} \end{cases} \tag{7}$$

and η is the surface roughness factor given by

$$\eta = \frac{\sigma_H \psi}{\lambda} \tag{8}$$

In (8), σ_H is the rms value of the sea wave height and λ is the wavelength of the microwave signal.

In practice, the received signal is contaminated with noise; i.e. the total received signal is

$$x_k = s_k + n_k \tag{9}$$

where n_k represents an arbitrary noise field.

In the RBF approach, the input/output relationship is modelled by a RBF neural network; i.e.

$$y(h) = \sum_{n=1}^{N} w_n \Phi_n(\|x - c_n\|) \tag{10}$$

where $\Phi_n(\|x-c_n\|)$ is a continuous function called the "basis function" and $\|\cdot\|$ denotes the norm in Euclidean space. The vectors c_n, n=1,..., N, are referred to as the centres of the basis functions. $\{w_n, n=1,...,N\}$ are the coefficients of the linear equation. For M snapshots of array inputs, a set of linear equations are formed based on (10)

$$\begin{bmatrix} y_1 \\ \cdot \\ \cdot \\ \cdot \\ y_M \end{bmatrix} = \begin{bmatrix} A_{11} & \cdot & \cdot & \cdot & A_{1N} \\ \cdot & \cdot & \cdot & \cdot & \cdot \\ \cdot & \cdot & \cdot & \cdot & \cdot \\ \cdot & \cdot & \cdot & \cdot & \cdot \\ A_{M1} & \cdot & \cdot & \cdot & A_{MN} \end{bmatrix} \begin{bmatrix} w_1 \\ \cdot \\ \cdot \\ \cdot \\ w_N \end{bmatrix} \tag{11}$$

where

$$A_{mn} = \Phi_{mn}(\|x_m - c_m\|) \tag{12}$$

and x_m is the mth snapshot data.

It turns out that a necessary condition for solving this optimization problem is the invertibility of the matrix **A**, and this condition is shown to be satisfied [6] if the p^{th} derivative of Φ is completely monotonic in $[0,\infty)$. One choice of such a function is the exponential function; i.e.

$$\Phi_n(\|x_m - c_n\|) = e^{-\frac{\|x_m - c_n\|}{\sigma}} \tag{13}$$

The target height corresponds to the value of h that gives the maximum response in the output $y(h)$.

There is one fundamental decision that needs to be made before the implementation of this technique. That is the determination of the centre vectors. The original RBF technique derived from the function approximation theory uses all of the multidimensional data as centres. However, this will form a huge matrix **A** which it is impractical to compute. Furthermore, the redundancy brought about by using all data points as centres may lead to misleading variations due to noise data. It was suggested in [7] that the number of centre vectors can be less than that of the input vectors. This results in a simpler non-square matrix. A least squared method can now be used to solve the matrix. The pseudo-inverse of **A** will provide a solution with the minimum least square errors. This optimum least square solution may be obtained either through direct evaluation of the pseudo-inverse **A** or through an adaptive algorithm such as the Least Mean Squares (LMS) algorithm or the Recursive QRD Least Squares algorithm [8].

In normal circumstances, the Gaussian nodes in a RBF network uses a constant in the

denominator of the exponent in (13). The constant σ should be determined a priori so that the estimation of the weights can be truly linear. In our case, we consider specific class of RBF networks, called classifying networks, in which a small value is assigned to σ in the exponent of the basis function. The approach of a classifying network is similar to that of the Pazen-window approach [2] which estimates the nearest neighbour of the input. Actually, the classifying network finds the input vectors that are the nearest neighbour of all the centre vectors in the hidden layer according to a distance measure. When a centre vector matches the input vector, the distance function is the smallest and the output of the Gaussian node of the of the RBF network, i.e. $\exp(-\|\cdot\|/\sigma)$, takes on its largest value. Each output represents the degree of closeness between the centre vector and the input vector. Classification is accomplished be finding the maximum among all the outputs. The constant σ serves as a sensitivity factor. If the σ is small, the hidden layer will be more sensitive to the fine changes in the distance function and discriminate against any other centre vector that is further away from the input vector.

3 Computer Simulations

In this section are presented the computer simulation results using synthetic radar signals which are assumed to have propagated through the troposphere with certain characteristics. The simulations were carried out to study (1) the error performance of the technique under various conditions and (2) the tracking performance of the technique for a moving target.

To start with, a simple simulation was conducted to test the algorithm's effectiveness in tracking a stationary target. For comparison purposes, the parameters used in this simulation were set to be exactly the same as those used in the experiments which are to be presented later. This simulation was based on one way propagation between a beacon operating at 10.2 GHz and a 32 element, 1.82 m aperture antenna array, which are 4.61 km apart. The synthetic data were generated based on (1) with SNR = 10 dB. The target height was chosen to be 9 m above the water surface, and one hundred trials were carried out. Then fifteen snapshots were grouped together to form a single target height estimate. Prior to processing, each signal vector was normalized with respect to the amplitude and phase at the top element of the array. Fig. 2 shows a trace of the height estimation. It is clear that the new technique can be used to track a target steadily with a high precision. The height estimates were always within 0.5 m of the actual

target height. The output spectrum in Fig. 3 demonstrates the algorithm's effectiveness in terms of its threshold and the accuracy with which it indicates the target height. The spectrum for the new technique has only one single sharp peak much like a delta function, rather than many ambiguous peaks which characterize the maximum likelihood approach using the same signal model [9].

One of the difficulties in processing the data is that the signal amplitudes and initial phases are unknown. One possible solution is to normalize the signal vectors with respect to the amplitude and phase of one of the array elements. However, it was observed that the performance depended on which element was used as the reference for the normalization. For optimal performance, it is suggested to respectively normalize the input signal vectors with respect to each element of the array and then to jointly process the normalized signal vectors [10]. As a simplified example of the the proposed normalization technique, we employed two references to carry out the normalization.

Three performance curves for the RBF network are shown in Fig. 4. The results corresponded to target heights 9m, 11m, and 15m, respectively. All the parameters were kept the same as before The mean square error (MSE) is calculated as followed

$$\mathscr{E} = \sum_{i=1}^{N_t} \frac{(h-\hat{h}_i)^2}{N_t} \tag{14}$$

where h is the true target height, $\hat{h}_i$ is the i^{th} estimate of h, and N_t is the total number of trials of ensembles to be averaged. In the case shown in Fig. 4, N_t was taken to be 100. Based on these results, the new technique shows promise. The performance threshold accounted for SNR values of less than 7 dB. For the case where h=11 m, it was as low as 5 dB.

We now consider the case where the low flying target is in motion. A simulation based on a single vertical moving target was used to demonstrate the true capability of the new method in tracking a single target over the range of the potential target heights. All the parameters were exactly the same as before, except that the target height was an exponential cosine function of time

$$h(t) = -20e^{\frac{t}{800}}\cos(\frac{\pi \cdot t}{600})+25 \quad (15)$$

There was no particular reason for choosing this function, rather than synthesizing a nonlinear motion for the target. In Fig. 5 are shown the tracking results. The corresponding SNR was set to be 15 dB. Again, 15 snapshots were used to derived an estimate. These 15 snapshots constituted a time window. In other words, a sliding window, consisting of 15 snapshots, was used as the estimates were derived. However, since the target height was a function of time, the 15 snapshots comprising a window corresponded to different heights. The dashed lines in Fig. 5 indicate the heights that corresponded to the first and last snapshots within the time window. It is then expected that the estimates should fall into the height interval marked by the dashed lines. Indeed, the results showed that this was the case.

In Fig. 6 is shown another case where SNR=12 dB. Once more, the tracking performance of the new algorithm was rather commendable, even though an outliner appears in the results. Outliners, however, can be removed by employing a Kalman filter or otherwise.

The advantages brought about by combining the deterministic multipath model with the RBF network are not only limited to high precision tracking at low SNR and the ability to trace a moving target. The simple parallelism behind the method also permits an easy implementation in a parallel processing computer. Besides, it does not require more than one training cycle nor the calculation of the inverse of a large matrix. Therefore, a real time processing is highly possible. The block diagram of the new low angle-tracking algorithm is illustrated in Fig. 7.

4 Real Data Experiment

In late October 1987, a series of experiments were performed on the west coast of the Bruce Peninsula, Ontario, Canada, overlooking Lake Huron. This particular location was chosen because of the high sea states caused by the combination of the westerly winds, the shallow water offshore, and the long fetch across Lake Huron. One of the objectives of these experiments was to acquire data suitable for elevating the performance of high-resolution estimation techniques for low-angle radar tracking applications. A 32-element sampled aperture antenna, developed at the Communications Research Laboratory, McMaster University, Hamilton, Ontario, Canada, was

used to collect multipath data under a variety of meteorological and water surface conditions. The experimental system consisted of a transmitter, a sampled aperture antenna, and a data acquisition system. The transmitter was a 100-mW CW beacon, sited at a distance of 4610 metres from the receiving antenna. The height of the transmitting horn could be varied through the height interval from 3.5 to 18.5 metres above the water level. The receiving antenna array has a 1.82-metre aperture and consists of 32 10-dB H-polarized horns. It follows from the geometry that the angular separation of the direct and reflected signals varied from 9% to 50% of a BW. All elements in the array were precisely aligned and uniformly distributed to within 0.1 mm to minimize errors due to placement of the antennas. The height of the centre of the sampled aperture antenna was fixed at 8.8 metres above the water level. The data were recorded with 12-bit precision at a sampling rate of 62.5 samples/second. The system operated at X-band.

Two sets of data were used to test the new algorithm. Each of the data sets contained 127 snapshots. The averaged amplitude and phase of the first data set were plotted along with those of synthetic data in Fig. 8 and Fig.4.9, respectively. The null which appears in the amplitude trace is due to the destructive interference between the direct and indirect signals. In this case, the best fit to the experimental data occurred for a the transmitter height of 9 m above the water surface and a sea wave-height-variation of 0.5 m. However, a large phase offset was observed between the synthetic signal and the measured signals. This difference is plotted in Fig 10. A linear relationship between the phase discrepancy and the location of the array element is observed. Thus, the error may be due to an imperfect calibration of the array or a tilt of the receiving array. In fact, the tilt meter that was mounted in the array was malfunctioned during the experiment. Therefore, the degree to which the array was tilted was unknown. Based on Fig. 10, it is speculated that the array was tilted upward. As well, the phase deviation observed for the 19^{th} element is another source of error. The defect may have been caused by a hardware failure for the 19^{th} element. It should be pointed out that these two errors were also present in a later data set.

For purposes of comparison, the MUSIC algorithm was also used to analyze the data. As mentioned before, the high correlation between the direct and the indirect signals will cause the MUSIC algorithm to fail in resolving the two incoming signals. In an attempt to reduce the correlation, the spatial smoothing technique was used with the array divided into ten subarrays.

The estimation results obtained using the MUSIC algorithm were shown in Fig. 11. Based on the experimental setup, the angular separation between the direct and indirect signals was approximately 0.4°. Therefore, it is easy to see that the MUSIC algorithm failed to resolve the two signals. There were two possible reasons for its failure. First, it was observed that the eigenvalue spread for the covariance matrix was large. This implies that a high degree of correlation still existed between the two signals after spatial smoothing. Second, the fact that the noise background was coloured degraded the MUSIC algorithm's resolving ability.

The new method, based on a deterministic multipath model and a nonlinear network, was used to process the data. Since we know a priori the two major sources of errors, the processing was carried out with and without corrections being made to the data. In Fig. 12 are shown three traces of tracking results. The first trace (the dotted line) was obtained without making any corrections to the data. The second trace (the dashed line) was obtained by omitting the signal at the 19th element. The last trace (the solid line) was obtained by not only omitting the signal at the 19th element, but also by adding a phase term to the data in order to compensate for the tilt of the array. In all three cases, the phase reference was chosen to be the 1st element and fifteen snapshots were grouped together to form a height estimate. Even though the first two cases contained corrupted data, the target was tracked to within a small range in height except at the end of the trace when the phase error of the 19th element became evident. The mean square tracking errors are 5.68 dB and 5.67 dB, respectively. The main source of this error was the false tracking (i.e. the trace jumping to another track) that occurred near the end of this result. Comparing these results with those obtained with the MUSIC algorithm, the nonlinear network demonstrated its superiority in providing a highly accurate angle-of-arrival estimates. The superiority was due to the fact that the new technique did not depend solely on the phase delay between the antenna elements. It also used both the amplitude and phase of the received signal. The first trace showed how the new technique has immunity to the phase error at the 19th element. In fact, the second trace was similar to the first one. Therefore, the major source of error in the estimates was due to the tilted array. The third experiment was successful in tracking the stationary target. The mean square error was -5.4 dB and the maximum error is 1 m.

Another set of measured data was also used to test the performance of the network in the same way. The target height for this data set was 15 m. The amplitude and the phase of the data were

compared with those of the synthetic data, as shown in Figs. 13 and 14. The phase difference between the measured and synthetic signals again exhibited a linear relationship with the array element, as shown in Fig. 15. The MUSIC algorithm, together with spatial smoothing using ten subarrays, was once again used to analyze the data and once again failed, as shown in Fig. 16. Similar to the previous set of measurement, the RBF network is able to provide a accurate estimate of the target height. These results are shown in Fig. 17. In the first trace (the dotted line), a few estimates were outliners. Since they did not appear in the second trace (the dashed line), which was obtained by omitting the signal from the false element, it was likely that the false estimates which appeared in the first trace were due to the phase error associated with this element. In the second trace, the height estimates fell into the neighbourhood of the true target height with a slightly larger bias than was the case for the third trace (the solid line). It seams clear that this small error was caused by tilt of the received antenna. For the solid-line trace, the means square error was -13.2 dB and the maximum discrepancy in target height was 0.2 m. Compared with the former data set, the height estimates in the second data set were less influenced by the phase error which was due to a defect element and dependant more on the amplitude of the signal. This may be related to the height of the target. When the target was located at 9 m, the incoming angle of the direct signal is slightly above the boresight of the antenna and the phase delay between the elements is almost negligible. Thus, it was more sensitive to changes of the phase delay.

The results derived from real-life data clearly demonstrate that the RBF network not only has the ability to track low flying targets under high sea-state conditions and correlated noise environments, but it is also less susceptible to other forms of errors such as phase errors due to imperfections in the antenna array. Furthermore, the new method offers very high performance in terms of resolution accuracy. In the two experiments, the largest deviation was less than one meter. Moreover, the performance of the new method was demonstrated to be robust in the sense that it did not depend on the nature of noise. This desirable attribute is due to the distance function used inside the radial basis function. The output of the RBF depended mainly on the Euclidean distance from the centre vectors. Therefore, it is insensitive to the characteristics of the noise.

5 Conclusions

In this paper, a new technique, based on a radial basis function neural network, has been developed as a solution to the low-angle tracking problem. Computer simulations were carried out to evaluate the performance of the algorithm. It has been shown, using simulated data, that the new technique was able to track both stationary and moving targets under low signal-to-noise ratio environments with high accuracy. It has also been demonstrated, using real-life multipath data, that the new technique is robust in the sense that it was its insensitive to array errors and the nature of the background noise. The algorithm is superior to the MUSIC algorithm in terms of robustness, resolvability, and estimation accuracy. On the other hand, more study is needed to understand how other factors, such as the centre vectors and coefficients used in the basis functions, affect the performance of the algorithm.

References

[1] E. Jakeman and R. J. A. Tough, "Statistical models of low-angle forward-scattering of microwaves," IEE conf. Publ. 281, Radar-87, pp 568-573, 1987.

[2] T.Poggio and F. Girosi, "Networks for approximation and learning," *Proc. IEEE*, vol.78, no.9, pp. 1481-1496, 1990

[3] R. P. Lippman, "An introduction to neural net," *IEEE ASSP Magazine*, pp. 4-22, April 1987.

[4] A. S. Lapedes and R. Farber, "Nonlinear signal processing using neural networks: Prediction and system modeling," Technical Report LA-UR-87, Los Alamos National Laboratory, 1987.

[5] T. Lo, J. Litva, "Low-angle tracking using multifrequency sampled aperture radar," *IEEE Trans. Aerospace and Electronic Systems*, vol. 27, pp.797-805, Sept. 1991.

[6] C. A. Miccelli, "Interpolation of scattered data: Distance matrices and conditionally positive definite functions," *Const. Approx.* vol. 2, pp. 11-22, 1986.

[7] D. S. Broomhead and D. Lowe, "Multivariable functional interpolation and adaptive networks," *Complex System*, vol. 2, pp. 321-355, 1988.

[8] S. Haykin, *Adaptive Filter Theory*, Prentice-Hall, 1991.

[9] E. Bosse, R. M. Turner, and M. Lecours, "Tracking swerling fluctuating targets at low altitude over the sea," *IEEE Trans. Aerospace and Electronic Systems*, vol. 27, pp.806-827, Sept. 1991.

[10] T. Wong, "Low-angle target tracking based on a deterministic multipath model and radial basis functions," M. Eng. Thesis, McMaster University, 1991.

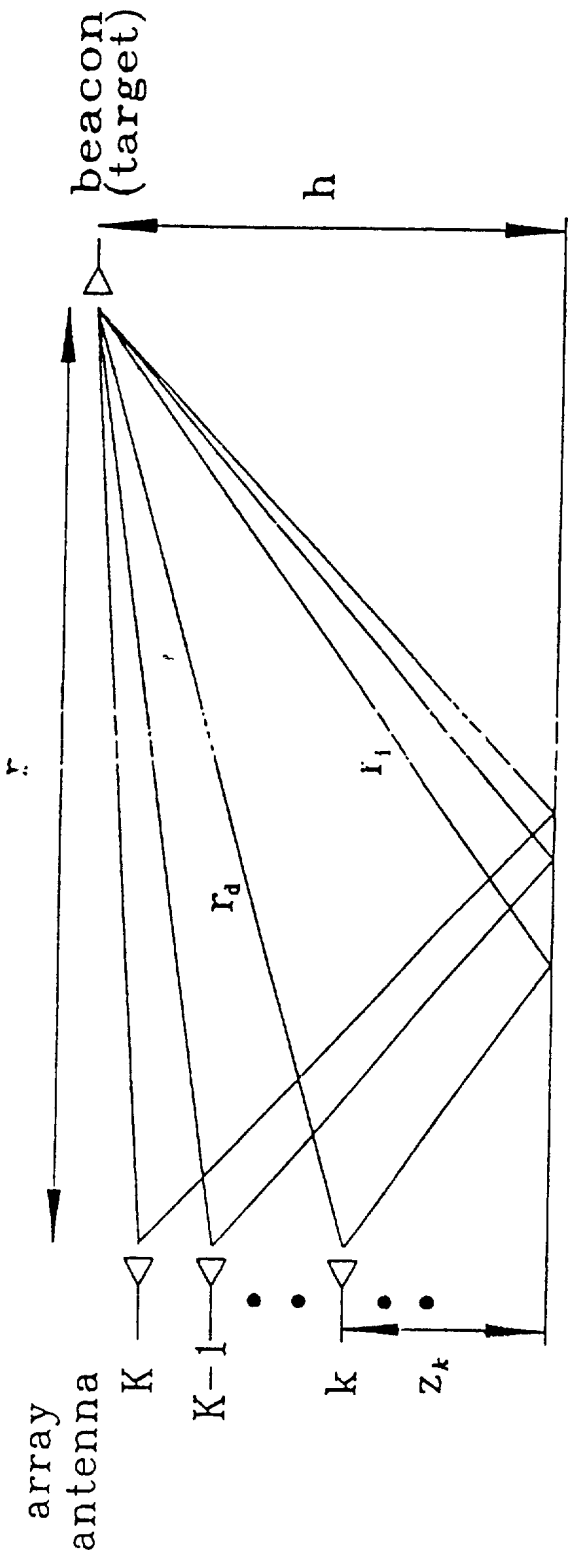

Fig. 1 Geometry of a simple flat-earth model for multipath.

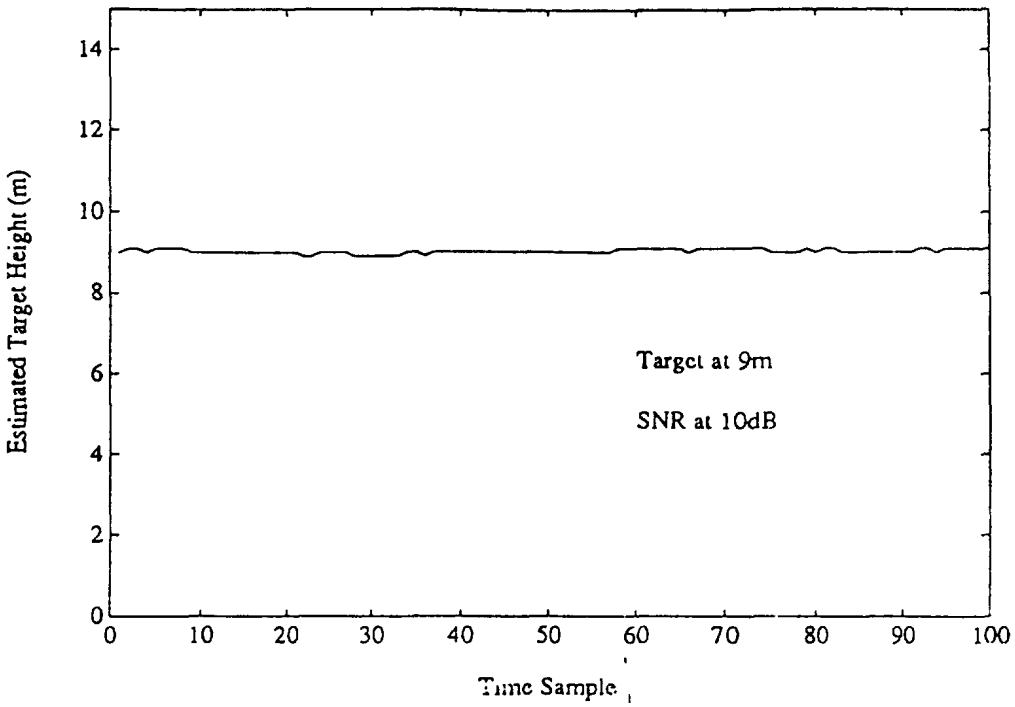

Fig. 2 A trace of target height estimates.

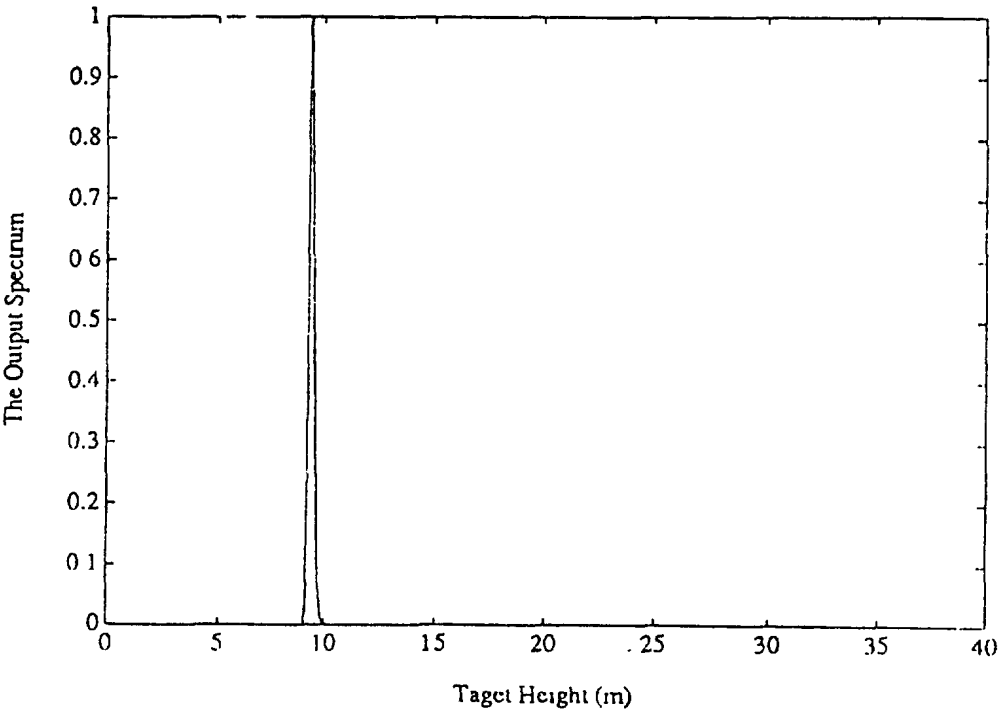

Fig. 3 The output spectrum of the RBF network.

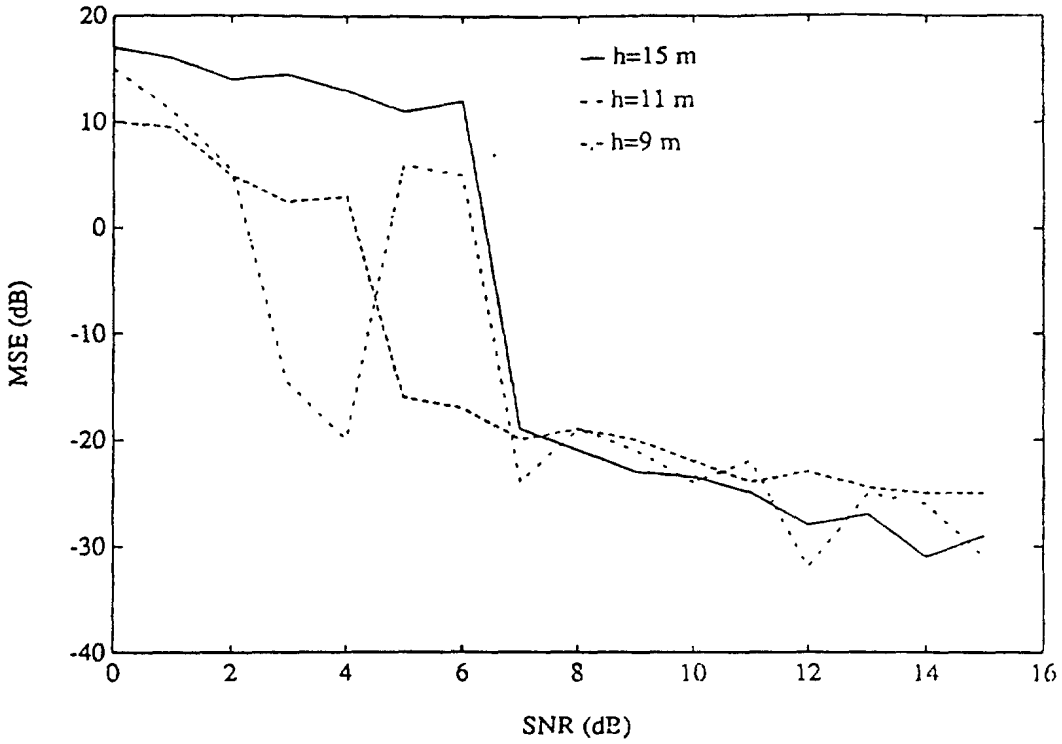

Fig. 4 The performance curves for the RBF network.

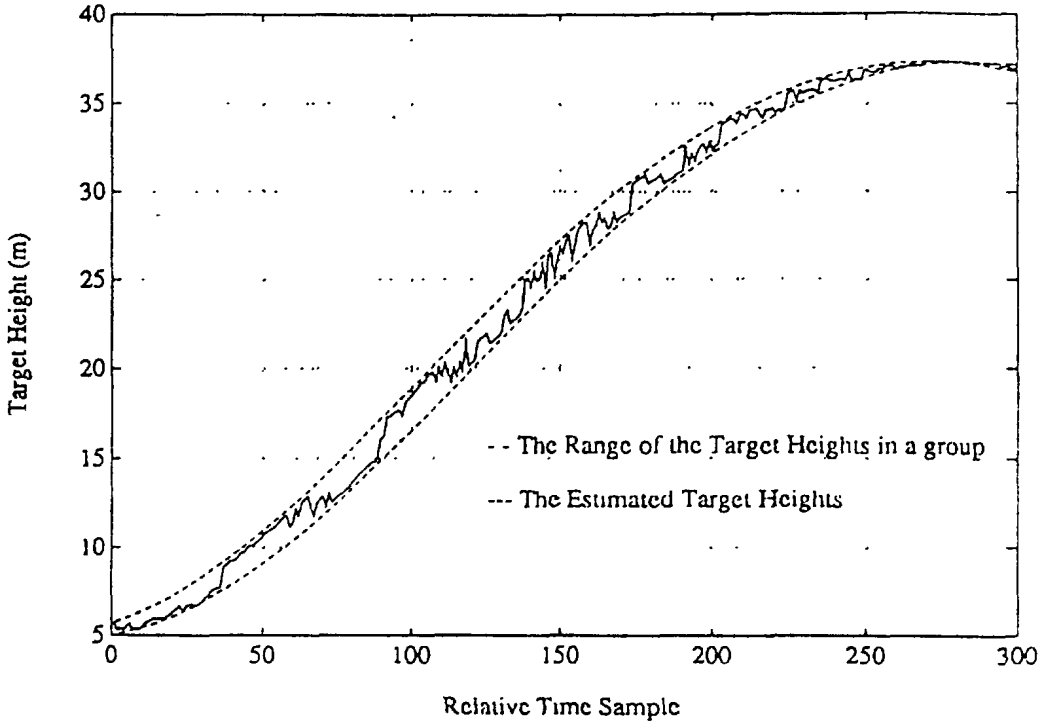

Fig. 5 The tracking results for a moving target; SNR=15 dB.

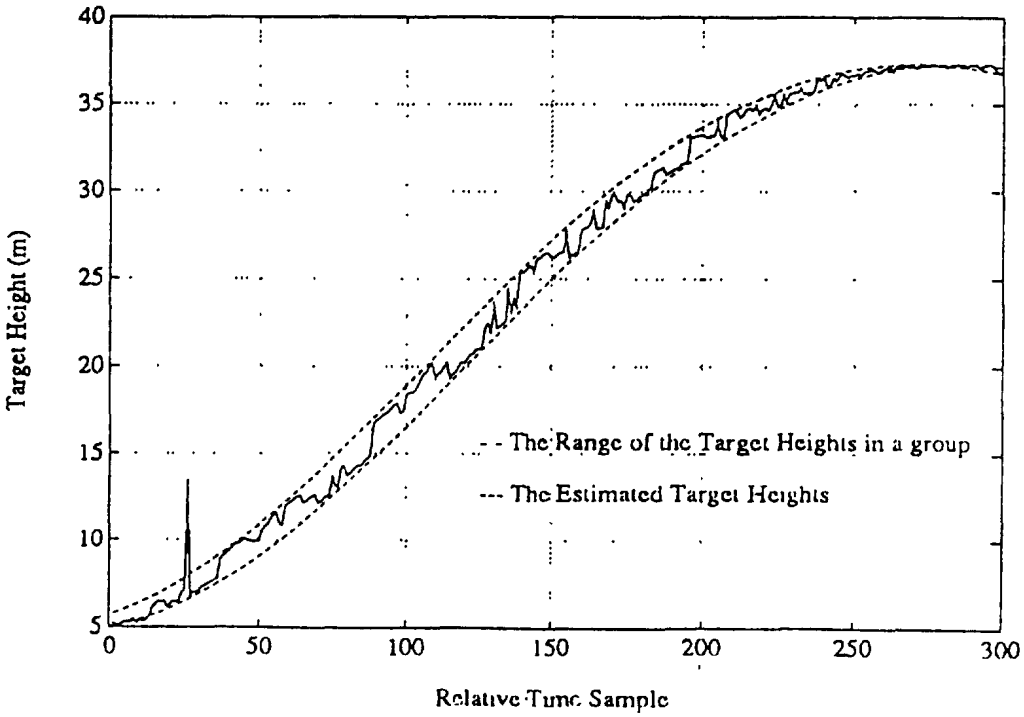

Fig. 6 The tracking results for a moving target; SNR=12 dB.

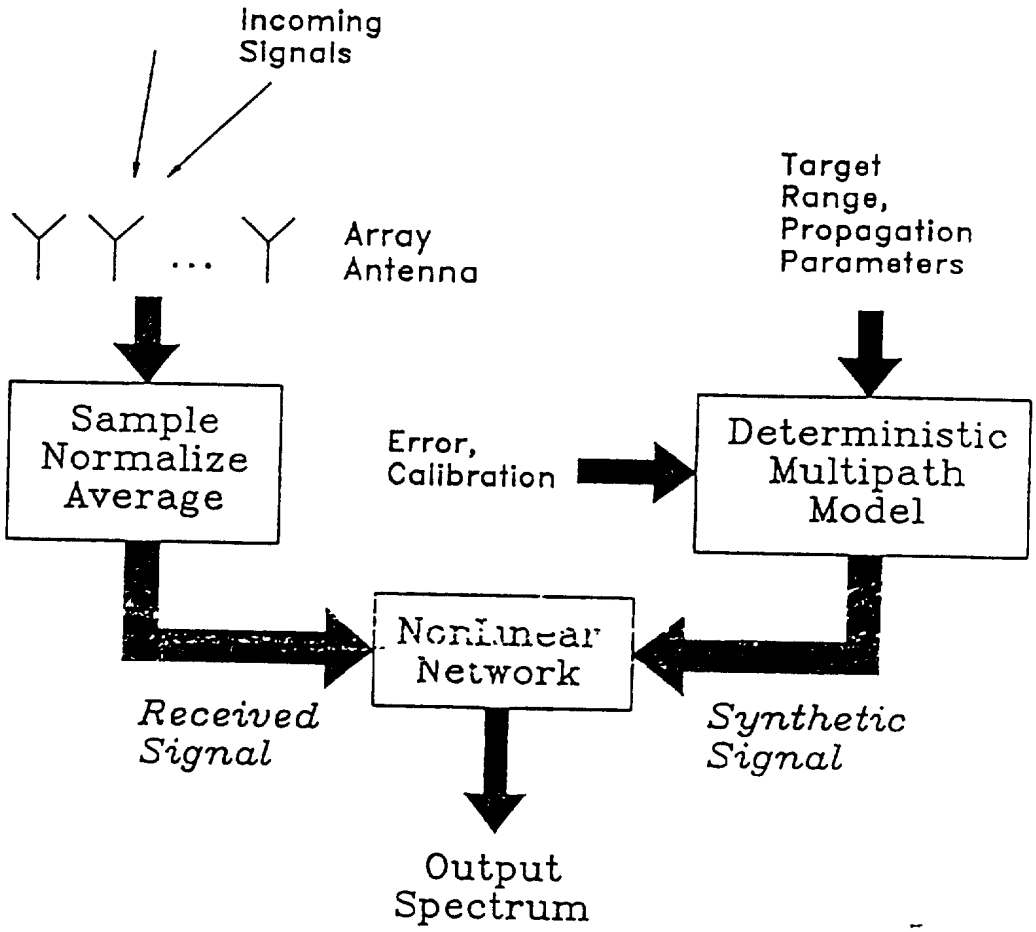

Fig. 7 Functional system diagram for implementing the RBF network.

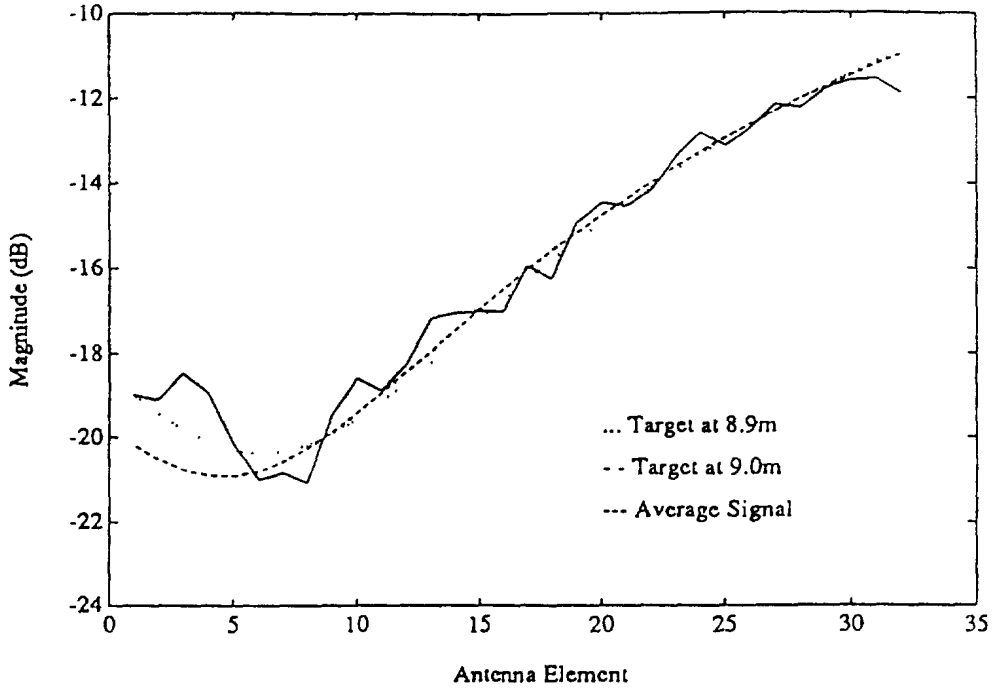

Fig. 8 Comparison of the amplitude distributions of synthetic data and the first set of the measured data along the array face

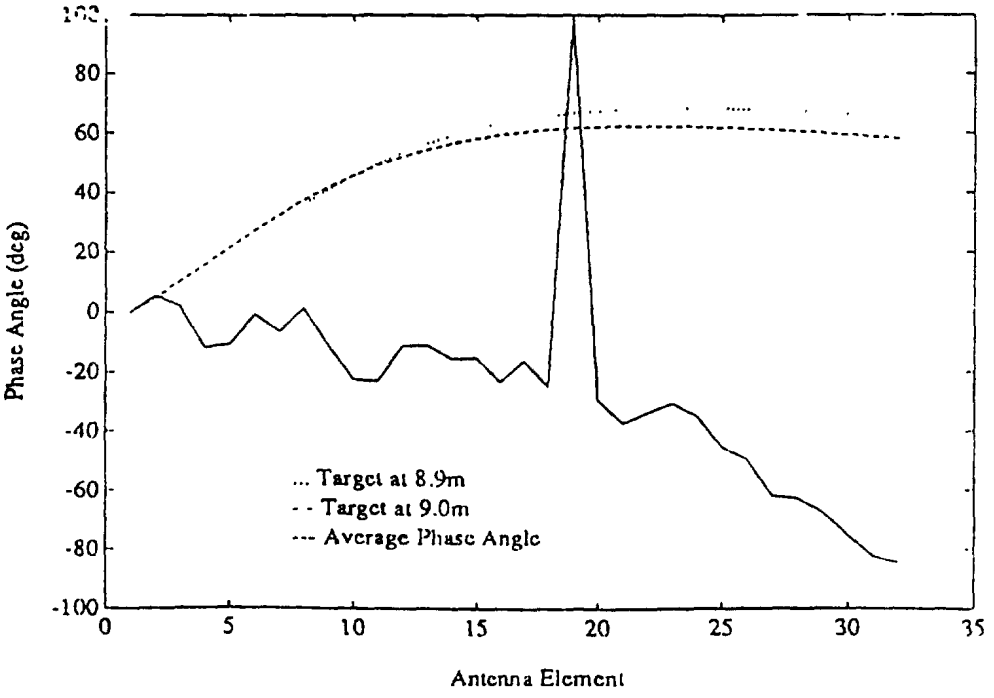

Fig. 9 Comparison of the phase distributions of synthetic data and the first set of the measured data along the array face.

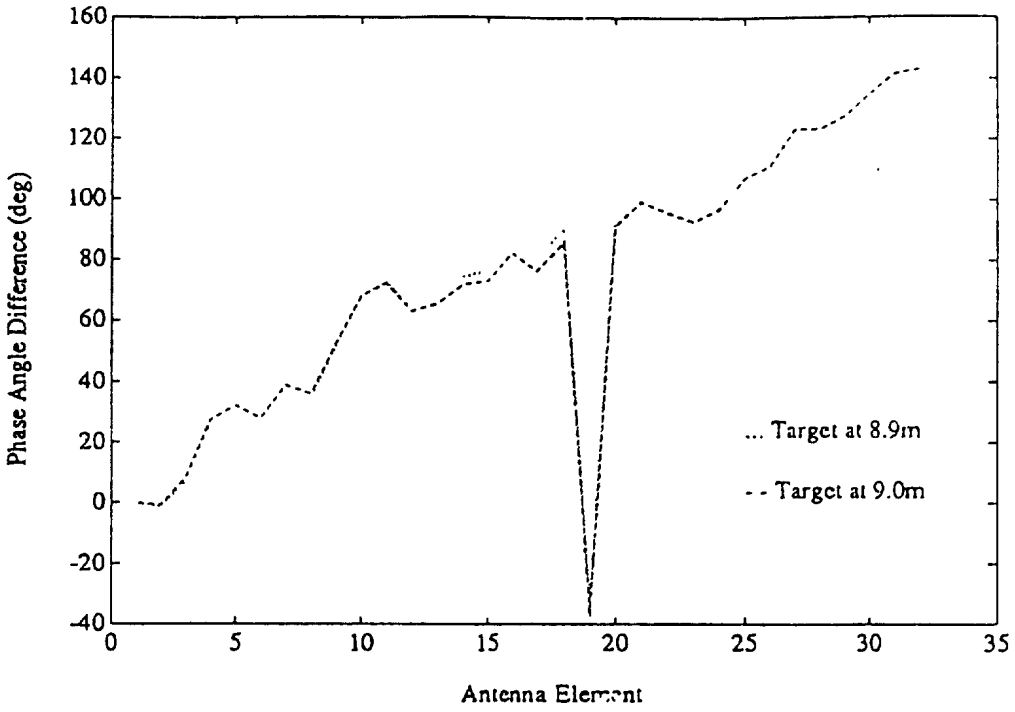

Fig. 10 Phase differences between the first data set and synthetic data.

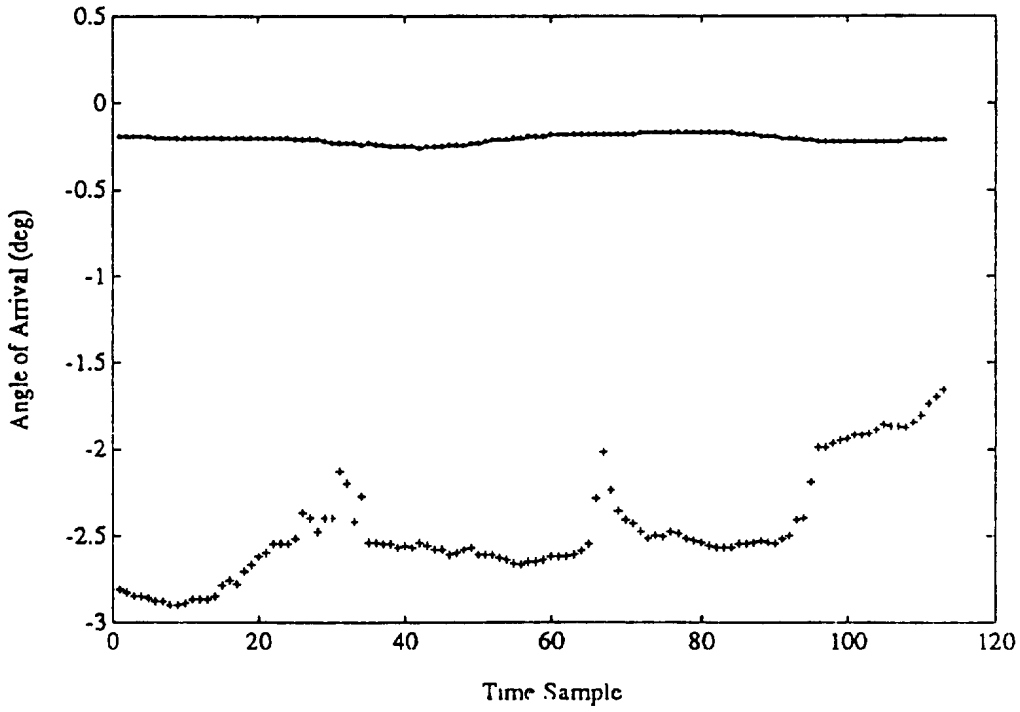

Fig. 11 The AOA results derived using the MUSIC algorithm.

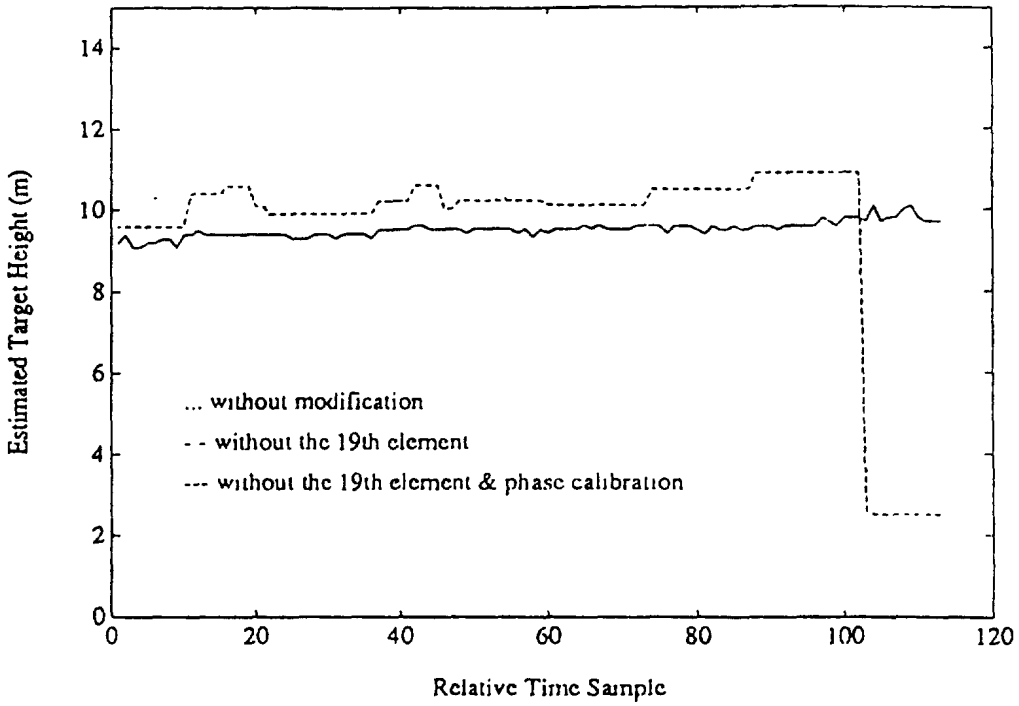

Fig. 12 The target height estimates obtained using the RBF network.

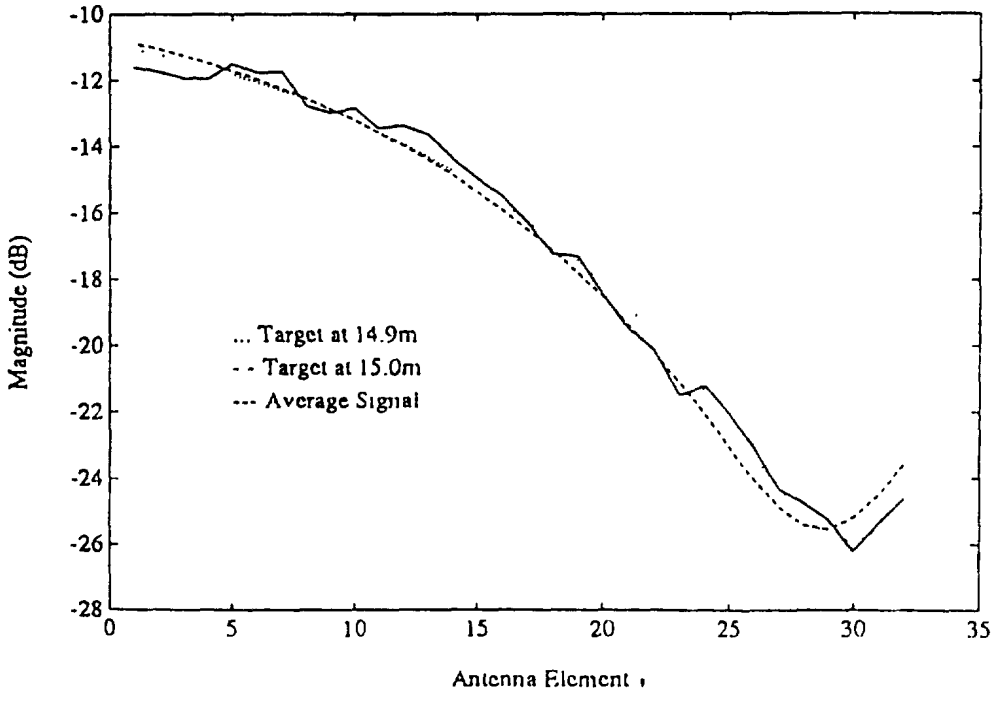

Fig. 13 Comparison of the phase distributions of synthetic data and the first set of the measured data along the array face

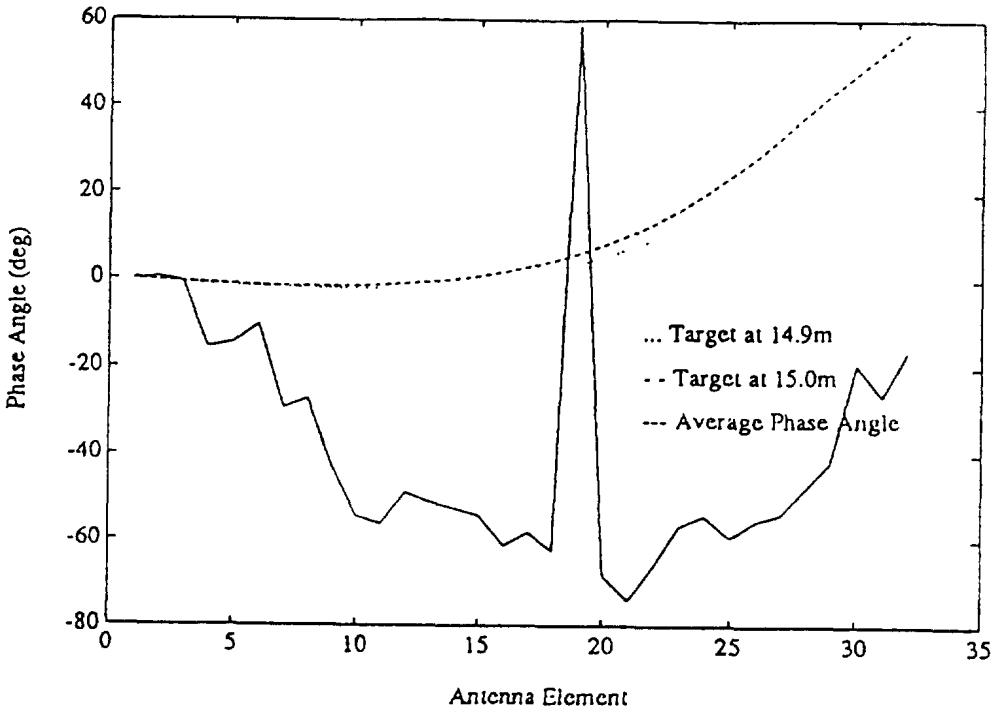

Fig. 14 Comparison of the phase distributions of synthetic data and the first set of the measured data along the array face.

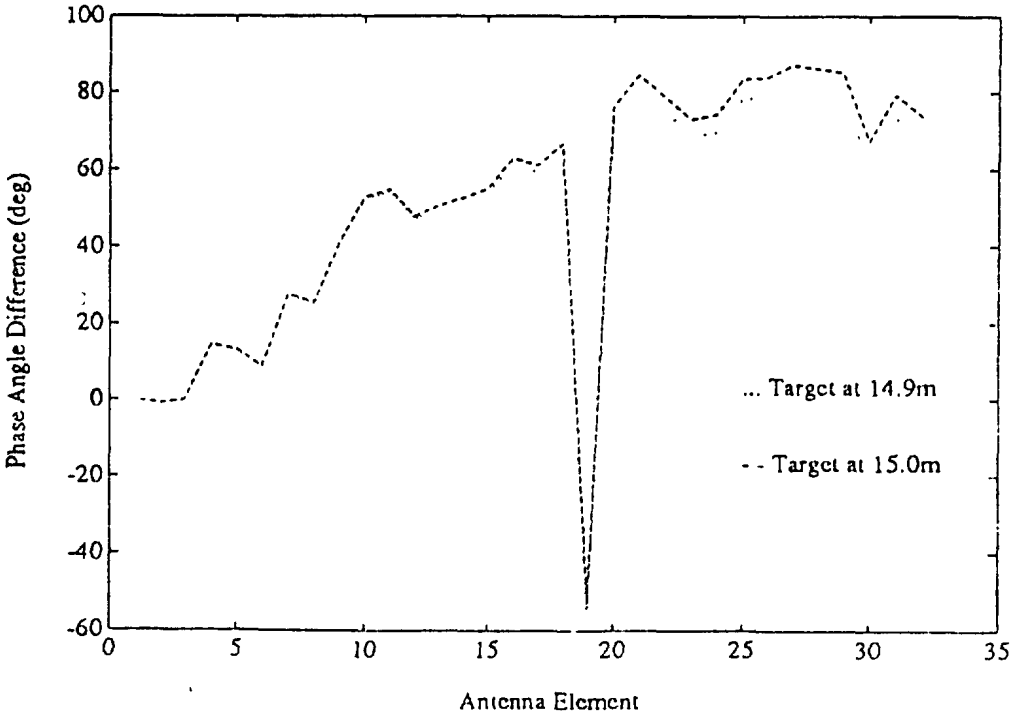

Fig. 15 Phase differences between the first data set and synthetic data.

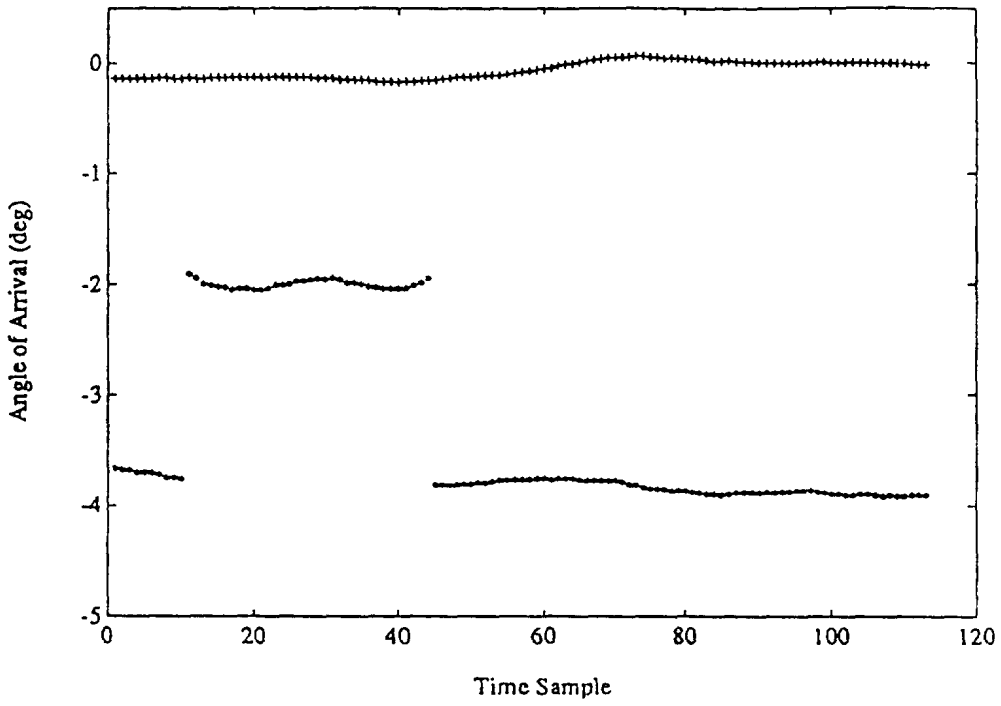

Fig. 16 The AOA results derived using the MUSIC algorithm.

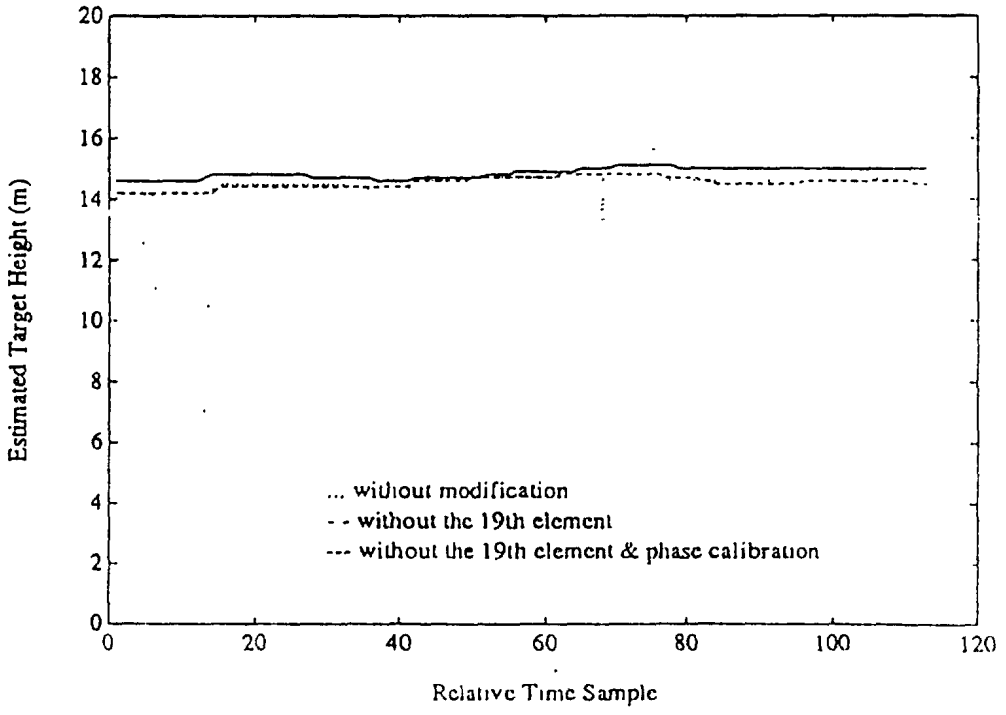

Fig. 17 The target height estimates obtained using the RBF network.